Available online at www.sciencedirect.com

SciVerse ScienceDirect

Ceramics International 38 (2012) 3999–4007

CERAMICS INTERNATIONAL

www.elsevier.com/locate/ceramint

Novel method of fabrication of polyaniline–CdS nanocomposites: Structural, morphological and optoelectronic properties

B.T. Raut [a], M.A. Chougule [a], Shashwati Sen [b], R.C. Pawar [c], C.S. Lee [c], V.B. Patil [a,*]

[a] Materials Research Laboratory, School of Physical Sciences, Solapur University, Solapur 413255, MS, India
[b] Crystal Technology Section, Technical Physics Division, BARC, Mumbai, India
[c] Division of Materials and Chemical Engineering, Hanyang University, Ansan 426-791, South Korea

Received 15 December 2011; received in revised form 10 January 2012; accepted 20 January 2012
Available online 28 January 2012

Abstract

Polyaniline–CdS nanocomposites have been synthesized by spin coating technique. The nanocrystalline CdS powder of particle size 40–50 nm was synthesized by sol–gel technique and the polyaniline was synthesized by chemical oxidative polymerization of aniline. The composite films were characterized by X-ray diffraction (XRD), field effect scanning electron microscopy (FESEM), Fourier transform infrared spectroscopy (FTIR), UV–Vis spectroscopy and Four probe method. The results were compared with corresponding data on pure polyaniline films. The intensity of diffraction peaks for PANi–CdS composites is lower than that for CdS. The conductivity measurement shows that molecular chain constitution of polyaniline is the most important carrier in polyaniline–CdS nano composite. The optical studies showed that variation in band gap of polyaniline (3.40 eV) to 2.54 eV CdS which is attributed to the interaction of CdS nanoparticles with PANi molecular chains.

Keywords: Polymers; Thin films; FESEM; Fourier transform infrared spectroscopy

1. Introduction

In recent years, the development of inorganic/polymer hybrid materials on nanometer scale has been receiving significant attention due to a wide range of potential applications in optoelectronic devices [1–3] and in field effect transistors [4]. The inorganic fillers at nanoscale exhibit high surface to volume ratio and thus expected to modify drastically the electrical, optical and dielectric properties of polymer. In general, the synthesis of hybrid of polymer/inorganic material has the goal of obtaining a new composite material having synergetic or complementary behaviors between the polymer and inorganic material. Polyaniline (PANi) is a most studied polymer because of its relative ease in preparation, good environmental stability [5–7] and tunable conductivity. Several reports on the synthesis of composite of nanofillers like: ZnO, CdS, Na^+-montmorillonite, Pd and Au with PANi have been demonstrated [8–12]. These synthesis processes have been carried out either in the aqueous solutions or via a sol–gel method, including the initial dispersion of the nanoparticles in the solution and the succedent oxidative polymerization of aniline with ammonium peroxidisulfate (APS). Since the conducting polyaniline and inorganic semiconducting material CdS in nano form both are having a wide range of technological applications, we got motivated to make composite of PANi and CdS and believed to get novel properties resulting from the molecular level interaction of these two dissimilar chemical components [12,13]. There are few reports on the synthesis of PANi–CdS composites for photovoltaic application [14,15]. However to the best of our knowledge no systematic study has been reported on structural, morphological, electron transport and optical properties of PANi–CdS nanocomposite.

In this paper we report the first time synthesis of PANi–CdS (10–50 wt%) nanocomposites films by spin coating technique and the study of their structural, morphological and optoelectronic properties.

2. Experimental details

2.1. Materials

Aniline (99%), hydrochloric acid (35% AR), ammonium peroxidisulfate (99%), methanol (99.8%) m-cresol (99%),

* Corresponding author. Tel.: +91 0217 2744771; fax: +91 0217 2744770.
E-mail address: drvbpatil@gmail.com (V.B. Patil).

0272-8842/$36.00
doi:10.1016/j.ceramint.2012.01.056

cadmium acetate (AR) and thiourea (AR) were purchased from Sd Fine Chem Ltd. Double distilled water was employed as a medium for the polymerization of aniline.

2.2. Synthesis of polyaniline (EB)

Polyaniline was synthesized by polymerization of aniline in the presence of hydrochloric acid (acts as a catalyst) using ammonium peroxidisulfate (APS) (acts as an oxidizing agent) by chemical oxidative polymerization method. For the synthesis, we took 2 ml of aniline and 1.0 M of HCl was added together in a 250 ml beaker with constant stirring at ≈0 °C. 4.9984 g of APS in 50 ml and 1.0 M HCl was suddenly added into the above solution. The temperature was maintained at ≈0 °C for 7 h to complete the polymerization reaction. After polymerization reaction, the resultant residual was filtered and washed successively by 1.0 M HCl followed by double distilled water repeatedly until the filtrate turned colorless. Then it was refiltered and washed again by double distilled water to get powder form of HCl-doped conductive polyaniline (emeraldine salt form). The HCl doped conductive polyaniline powder was insoluble in any organic solvent so it was treated with ammonia solution (NH_4OH) to get undoped polyaniline (emeraldine base form) which was soluble in organic solvent like m-cresol The undoped polyaniline was washed with methanol to remove the oligomers and the residual was dried in oven at 60 °C for 24 h and ground in pestle mortar to get an undoped polyaniline in powder form For thin film formation, the undoped polyaniline (EB) powder was dissolved in m-cresol. The solution was stirred for 11 h and filtered with a Whatman filter paper having pores of size of few microns. A film of this filtered undoped PANi was deposited by spin coating method on a glass substrate with 3000 rpm for 30 s and dried on a hot plate at 100 °C for 10 min [16,17].

2.3. Synthesis of nanocrystalline CdS

Nanocrystalline CdS powder has been synthesized by a sol–gel process in which cadmium acetate ($Cd(CH_3\ COO)_2{\cdot}2H_2O$) has been used as a parent source for Cd and thiourea (CH_4N_2S) has been used as a source of S. For experiment, 3.198 g of cadmium acetate and 1.824 g of thiourea was added into 40 ml of methanol and mixture was stirred vigorously at 60 °C for 1 h (gel formation). After gel formation heating was stopped and the solution was stirred continued until we get a yellow powder. The powder was dried in zone furnace at 300 °C for 30 min to get the nanocrystalline CdS powder having particles of size of 40–50 nm.

2.4. Synthesis of PANi–CdS nanocomposite

The nanocomposites of CdS with undoped PANi (EB) were prepared by adding CdS in weight percentage (10–50%) into PANi (EB) matrix in m-cresol and stirring it for 11 h. Films of the nanocomposite were prepared on glass substrate by spin coating method at 3000 rpm for 30 s.

2.5. Characterization techniques

X-ray diffraction (XRD) studies were carried out using a Philips powder X-ray diffractometer (Philips – PW 3710 (Almelo, Holland)). The XRD patterns were recorded in the 2θ range of 20–80° with step width 0.02° and step time 1.25 s using CuK_α radiation ($\lambda = 1.5406$ Å). The XRD patterns were analyzed by matching the observed peaks with the standard pattern provided by JCPDS file. Fourier Transform Infra Red (FTIR) spectroscopy (Model: Perkin Elmer 100, Santa Clara, CA, USA) of PANi, CdS and PANi–CdS (10–50%) nanocomposites were studied in the frequency range of 400–4000 cm^{-1}. Morphological study of the films of PANi and PANi–CdS composite was carried out using scanning electron microscopy (FESEM Model: JSM JEOL 6701F, Tokyo, Japan) operating at 20 kV. UV–Vis spectra of the samples, which were dispersed in de-ionized water under ultrasonic action, were recorded on a Simandzu-100 UV–Vis spectrophotometer (Kyoto, Japan). The dc electrical conductivity measurements were made on CdS, PANi (EB) and PANi–CdS (10–50%) thin films using custom designed two probe techniques. Thermoelectric power measurements for CdS, PANi (EB) and PANi–CdS (10–50%) thin films were carried out using custom designed thermoelectric power unit in 300–500 K temperature range. The thickness of the CdS, PANi (EB) and PANi–CdS (10–50%) thin films was measured using AMBIOS make XP^{-1} surface profiler with 1 Å vertical resolution and weight difference method. Fig. 1 shows flow diagram of synthesis and deposition of PANi–CdS nanocomposite.

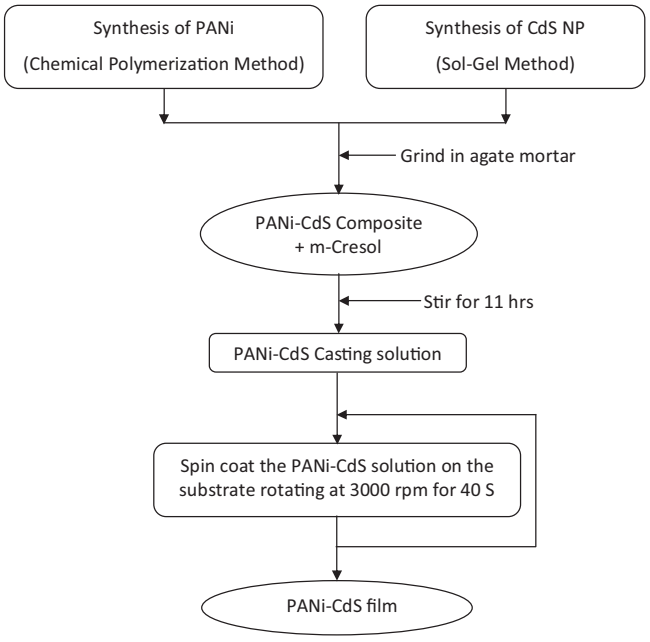

Fig. 1. Flow diagram of synthesis and deposition of PANi–CdS nanocomposites.

Table 1
Thin film properties of PANi–CdS (10–50%) nanocomposite.

Sr. No.	Composition	Thickness (μm)	Crystallite size, (nm, from XRD for [0 0 2] plane)	Energy gap, E_g (eV)	Activation energy, $E_{a\sigma}$ (eV)		Carrier concentration, n ($\times 10^{19}$ cm^{-3})	Mobility, μ ($\times 10^{-5}$ cm^2, V^{-1} s^{-1})	Barrier potential Φ_B (eV)
					HT	LT			
1	PANi (EB)	0.92	72	3.42	0.66	0.18	2.1	3.7	0.45
2	CdS	0. 76	42	2.54	0.46	0. 11	4.2	1.4	0.62
3	PANi–CdS (10%)	0.89	49	3.24	0.48	0.10	2.2	3.4	0.46
4	PANi–CdS (20%)	0.87	51	3.07	0.53	0.12	2.4	3.1	0.48
5	PANi–CdS (30%)	0.84	58	2.98	0.55	0.14	2.45	2.9	0.51
6	PANi–CdS (40%)	0.82	61	2.87	0.58	0.12	2.48	2.7	0.53
7	PANi–CdS (50%)	0.79	64	2.69	0.61	0.16	2.5	2.4	0.56

3. Results and discussion

3.1. Growth mechanism and film formation

3.1.1. For CdS

The growth mechanism of CdS film formation by the sol gel spin coating method can be enlightened as follows:

$$Cd(CH_3COO)_2{\cdot}2H_2O + 2CH_3{-}OH \rightarrow Cd(OH)_2 + 2CH_3COOCH_3 + 2H_2O$$

$$CH_4N_2S + 2CH_3{-}OH \rightarrow CHS^{2-} + 2CH_3N + 2H_2O$$

Since to improve crystallinity and remove hydroxide phase, powder was annealed at 200 °C for 1 h pure CdS is formed after air annealing by following mechanism:

$$Cd(OH)_2 + CH\quad S^{2-}\downarrow + \text{carbonaceous compounds} \xrightarrow[\text{oxidation}]{\text{air annealing}} CdS + H_2O\uparrow$$

Thin films of CdS are formed using m-cresol solvent. The deposited CdS films were found to be strongly adhering to the glass substrate and they appeared in orange color.

3.1.2. For PANi and PANi–CdS

The proposed mechanism of formation of PANi and PANi–CdS formation by chemical polymerization method can be enlightened as follows:

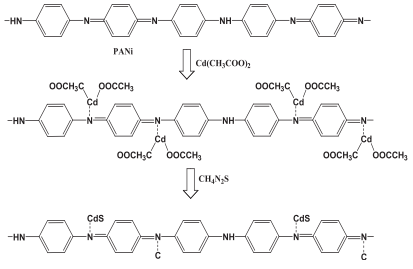

The deposited films of PANi (EB), PANi–CdS nanocomposites were found to be strongly adhering to the glass substrate and they appeared in dark green and lime color respectively. The thickness of CdS, PANi (EB), PANi–CdS nanocomposites films (10–50%) on the glass substrate was calculated using gravimetric weight difference method using formula:

$$t = \frac{m}{A\rho} \quad (1)$$

where t is film thickness of the film; m is actual mass deposited onto substrate; A is area of the film and ρ is the density of CdS (4.83 g/cm^3) and PANi (1.30 g/cm^3). The thickness of CdS, PANi (EB) and PANi–CdS (10–50%) films also confirmed by surface profiler and no much change is observed in both measurements. The optimized thicknesses are given in Table 1.

3.2. Structural analysis of PANi, CdS and PANi–CdS nanocomposites

Fig. 2 shows the XRD patterns of pure polyaniline in the emeraldine base form, cadmium sulfide (CdS) and PANi–CdS nanocomposites (10–50 wt%). The XRD pattern of PANi shows a broad peak at $2\theta = 25.30^\circ$ which corresponds to (1 1 0) plane of PANi [16,17]. This broad peak in the XRD pattern of PANi shows that it has some crystallinity. The crystallinity of PANi can be ascribed to the repetition of benzenoid and quinoid rings in PANi chains [18]. The XRD patterns of nano CdS, PANi–CdS (10–50 wt%) nanocomposites exhibit the characteristic peaks for crystalline CdS of hexagonal wurtzite structure. This indicates the crystal structure of CdS is not modified due to the presence of PANi. The diffraction peaks in XRD patterns of nano CdS powder and PANi–CdS (10–50 wt%) nanocomposites have been indexed to the hexagonally wurtzite structured CdS which are consistent with the standard values for CdS given in JCPDS file (80-006). All the diffraction peaks of nanocrystalline CdS were found to shift to lower 2θ values in PANi–CdS (10–50 wt%) nanocomposites. The lattice constants for prominent XRD peak (0 0 2) plane of hexagonal CdS in PANi (EB)–CdS (10–50%) nanocomposites were calculated using standard formula for determination of lattice constants of hexagonal system and the values obtained are $a = b = 4.189$ Å, $c = 6.706$ Å. The values of lattice constants agree well with standard hexagonal CdS system (JCPD No. 80-006). Slight increase in lattice constants of CdS was found in PANi–CdS (10–50 wt%) nanocomposites. The increase in lattice parameters indicates a slight stretching of unit cell of

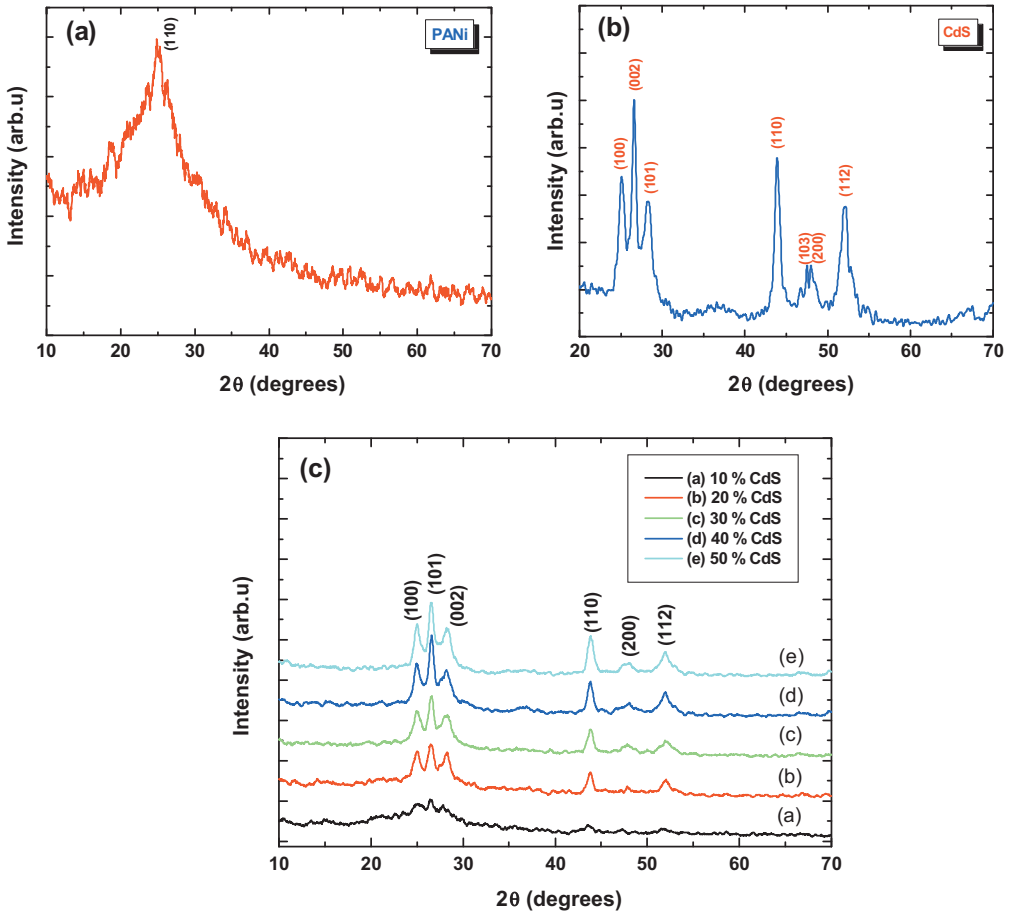

Fig. 2. X-ray diffraction pattern of (a) PANi (EB), (b) CdS and (c) PANi–CdS (10–50%) nanocomposites.

CdS due to the adsorption of PANi molecular chains on the surface of the CdS. The presence of such interaction can also be studied by the change in crystal size of prominent peaks (0 0 2) planes of X-ray diffraction pattern of PANi–CdS nanocomposites. The crystallite sizes of CdS, PANi–CdS (10–50 wt%) nanocomposites for prominent peaks (0 0 2) are calculated by Scherrer formula and are given in Table 1. The crystallite sizes of CdS in (0 0 2) planes increase from 49 nm to 64 nm in PANi–CdS (10–50 wt%) nanocomposites. Increase in crystallite sizes of CdS in PANi–CdS (10–50 wt%) nanocomposites shows that the crystallinity of CdS is disturbed by the adsorption of PANi molecular chains on the surface of CdS. These results indicate the interaction between the CdS nano particles and PANi molecular chains due to the adsorption of PANi molecular chains on the surface of the CdS.

3.3. Fourier transform infrared analysis

Fig. 3 represents the FT-IR spectra of PANi (EB), nano CdS and PANi (EB)–CdS nanocomposites and the peak locations related to the corresponding chemical bonds are listed in Table 2 and are in good agreement with those reported in the literature [19].

Fig. 3(a) shows FT-IR spectra of the undoped PANi (EB). The characteristic absorption peaks of PANi (EB) at 1560 cm^{-1}, 1457 cm^{-1}, 1287 cm^{-1}, 1125 cm^{-1} and 801 cm^{-1} correspond to the C=N imino quinone, C=C stretching mode of quinoid rings, the C=C stretching mode of the benzenoid rings, the stretching mode of C–N, the stretching mode of N=Q=N where Q represents the quinoid ring and C–H bonding mode of aromatic rings [20,21]. FTIR spectra of nano CdS are shown in Fig. 3(b). The band at 3827 cm^{-1} is due to OH stretching vibrations of water molecules. The bending vibrations of water molecules appeared at 2054 and 1636 cm^{-1}, C–C stretching, CdS particles showed two stretching bands, asymmetric and symmetric, at 3334 cm^{-1} and 3145 cm^{-1}, associating with C–H stretching [22]. At 614 cm^{-1} and 793 cm^{-1}, there are medium to strong bands which have been assigned to Cd–S stretching [23].

Fig. 3(c) shows FTIR spectra of PANi–CdS (10–50%) nanocomposite. In the spectra, presence of the bands at 1500 and 1600 cm^{-1} in all the PANi–CdS nanocomposites shows that the intensity of bands in polymer due to amine and imine groups has decreased. This could be due to the presence of different oxidation states of polymers. Similarly, the shifts in aromatic peaks that is C–H stretching mode of vibrations is also observed which is consistent with the values that are normally observed for PANi (EB). In the present case the C–H absorption frequency has shifted by about 20 cm^{-1} from its well reported value of about 3000 cm^{-1} and is found at 3017 cm^{-1}, a further shift from 2992 cm^{-1} in PANi (EB). A comparison of FTIR values of PANi (EB), CdS and PANi (EB)–CdS nanocomposites is shown in Table 2. From the table it can be seen that

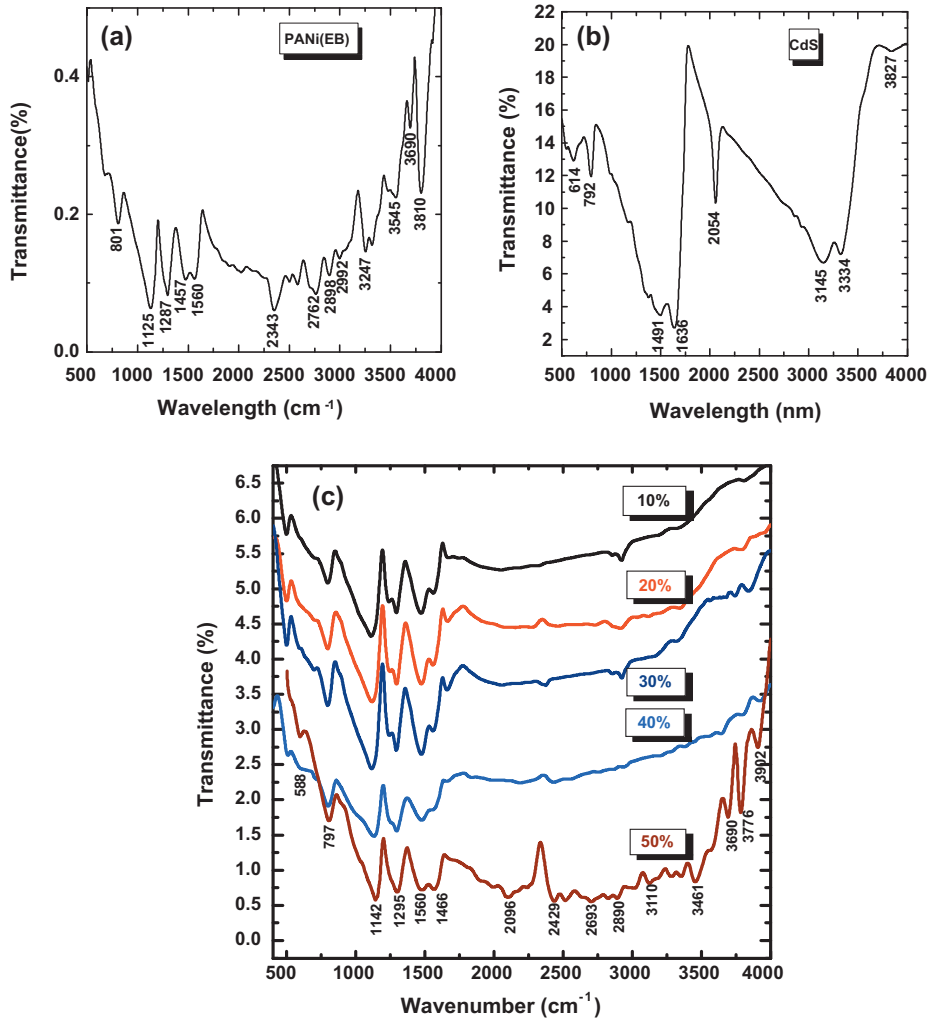

Fig. 3. FTIR of (a) PANi (EB), (b) CdS and (c) PANi–CdS (10–50%) nanocomposites.

almost all absorption values have shifted to either higher or lower values in case of composite with CdS. This indicates that nano-sized CdS has affected the absorption phenomena in the IR region for the composite.

Table 2
A comparison of FTIR values of PANi (EB), CdS and PANi (EB)–CdS nanocomposites.

CdS position (cm^{-1})	PANi (EB) position (cm^{-1})	PANi–CdS position (cm^{-1})	Assignment
614	–	588	Cd–S stretching (medium)
792	–		Cd–S stretching (strong)
–	801	797	Paradisubstituted aromatic rings indicating polymer formation
–	1125	1142	C–H in plane bending vibration
–	1287	1295	Aromatic C–N stretching indicating secondary aromatic amine group
–	1457	1466	C–N stretching of benzoid rings
–	1560	1560	C–N stretching of quinoid rings
–	2992	3017	The aromatic C–H stretching
–	3247	3264	N–H stretching vibrations

3.4. Morphological analysis of PANi, CdS and PANi–CdS nanocomposites

Fig. 4(a), (b) and (c)–(g) shows the field emission scanning electron (FESEM) micrographs of PANi (EB), CdS and PANi–CdS (10–50 wt%) films. The FESEM image of the polyaniline film (Fig. 4(a)) exhibits a nanofibrous structure with many pores and gaps among the fibers. Fig. 4(b) shows the surface morphology of the CdS nanoparticles. The image shows that the nanoparticles are glued each other. The image of the PANi–CdS (10–50 wt%) nanocomposite (Fig. 4(c)–(g)) shows that CdS nanoparticles are glueded into nanofibrous morphology of PANi (EB) matrix. It was considered that the nanostructured CdS particles embedded within the netlike structure built by PANi chains.

3.5. Optical properties PANi, CdS and PANi–CdS nanocomposites

The optical absorption spectrum PANi, CdS and PANi–CdS (10–50 wt%) nanocomposites were obtained and studied to evaluate the absorption coefficient (α) energy gap (E_g) and nature of transition involved. It is found that the optical

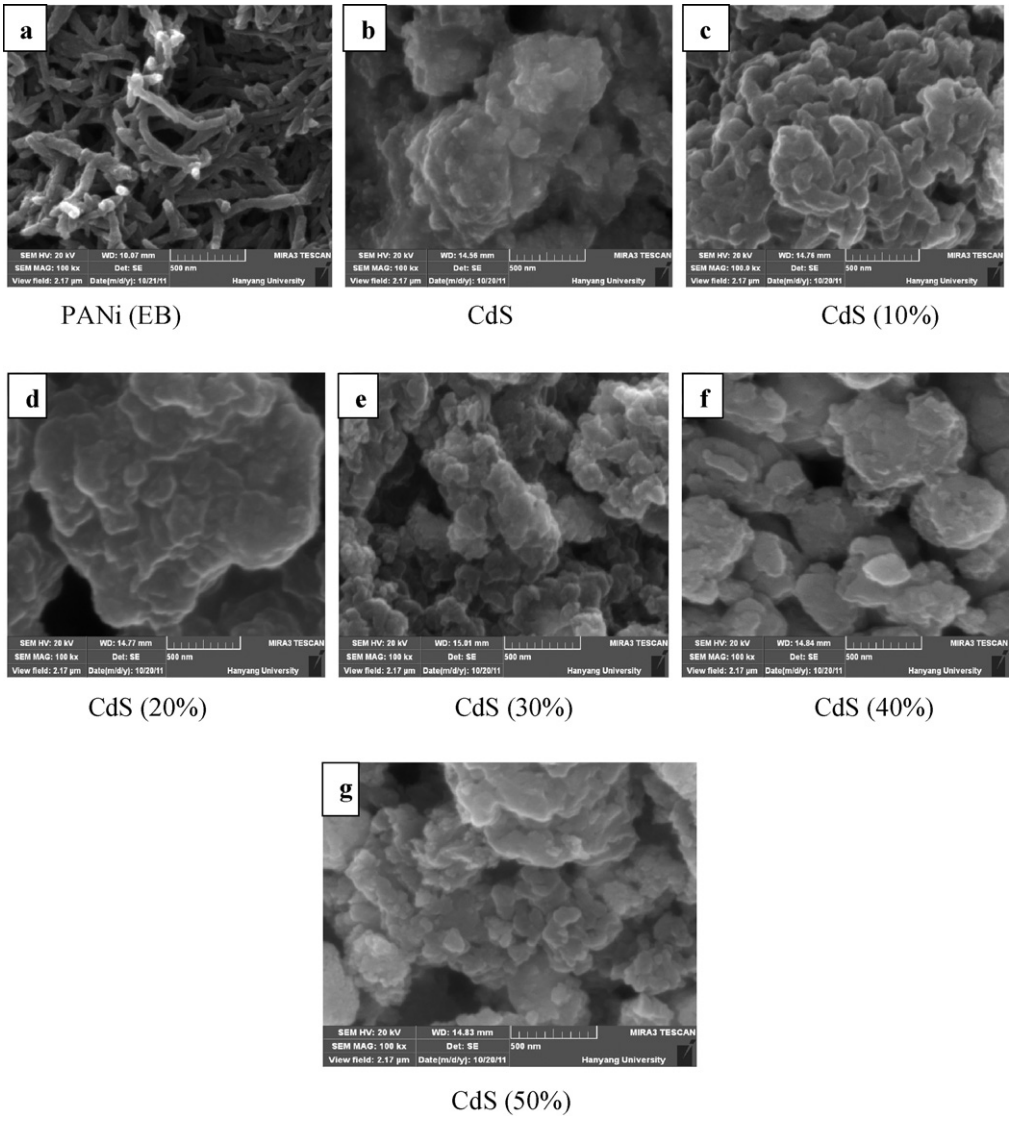

Fig. 4. FESEM images of (a) PANi (EB), (b) CdS and (c) PANi–CdS (10–50%) nanocomposites.

absorption coefficient is higher for all the composites (10^4 cm^{-1}). The absorption coefficient (α), energy gap (E_g) and photon energy ($h\nu$) are related as [24,25]:

$$\alpha h\nu = A(h\nu - E_g)^{n/2} \quad (2)$$

Assuming the mode of transition to be of the direct allowed type ($n = 1$), the band gap energies have been calculated from the variation of $(\alpha h\nu)^2$ versus $h\nu$ (Fig. 5). The $(\alpha h\nu)^2$ versus $h\nu$ plots shows straight line behavior on the higher energy side that confirms direct type of transitions involved in these films. It is also seen from Fig. 5, that the band gap is decreased typically from 3.40 eV (pure PANi (EB)) to 2.54 eV (for CdS) as content of CdS nanoparticles increased from 0 to 50%. The band gap of CdS in present case is 2.54 eV was observed due to formation of nanosized cadmium sulfide. This change in band gap of CdS indicated a blue shift by about (0.12 eV) with respect to the bulk CdS that is reported to have band gap of 2.42 eV [26]. The blue shift is due to the size quantization [27,28] and is observed when there is an increase in the band gap energy between the lowest unoccupied molecular orbital's (LUMO) and highest occupied molecular orbital's (HOMO) in semiconductors.

The mode of optical transition in PANi, PANi–CdS (10–50 wt%) nanocomposites and CdS has been confirmed from the variation of $\ln(\alpha h\nu)$ versus $\ln(h\nu - E_g)$ (Fig. 6) which showed 'n' nearly equal to 1 indicating direct type of transition.

3.6. Electrical transport properties of PANi, CdS and PANi–CdS nanocomposites

The dc electrical conductivities of PANi (EB), CdS and PANi–CdS (10–50 wt%) nanocomposites were measured in the 300–500 K temperature range and their temperature dependence can be fitted to a usual Arrheneous equation:

$$\sigma = \sigma_o \exp\left(\frac{-E_{a\sigma}}{KT}\right) \quad (3)$$

where $E_{a\sigma}$ is the conductivity activation energy.

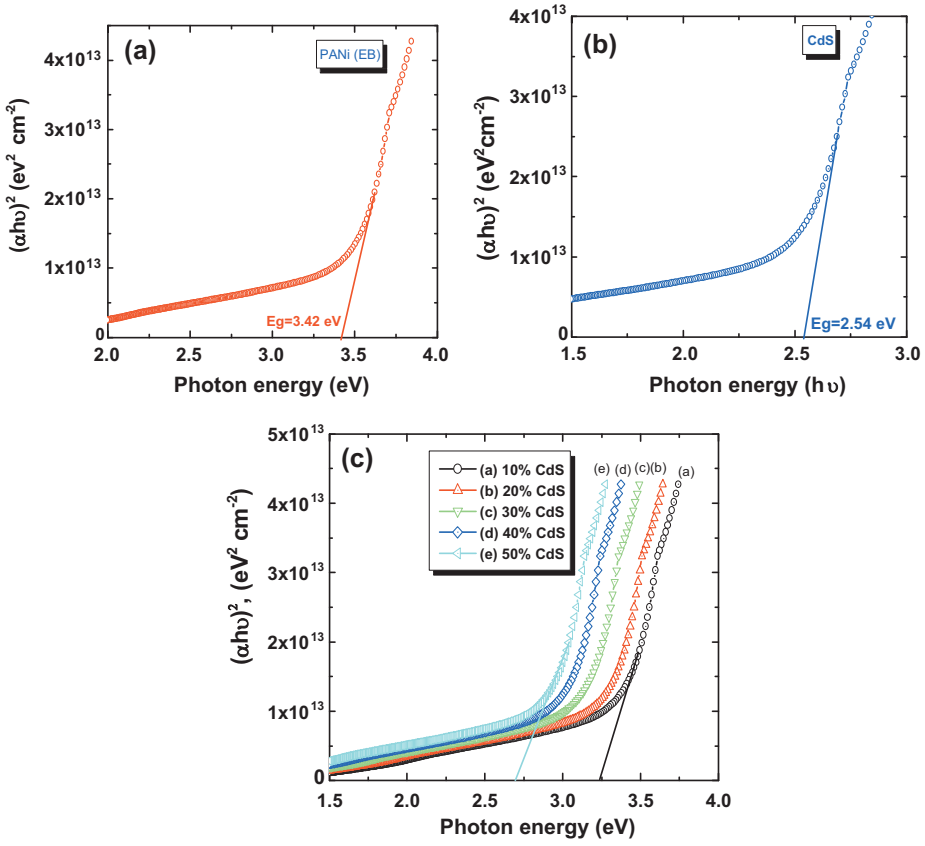

Fig. 5. Plot of $(\alpha h\nu)^2$ versus $h\nu$ (a) PANi (EB), (b) CdS and (c) PANi–CdS (10–50%) nanocomposites.

The temperature dependence of dc electrical conductivity of PANi (EB), CdS and PANi–CdS (10–50 wt%) (Fig. 7) showed two distinct conduction regions corresponding to two different conduction mechanisms; one, a grain boundary scattering limited and second a variable range hopping [29]. The activation energies of an electrical conduction have been computed for both regions and it is ranged between 0.44 and 0.52 eV.

The room temperature dc electrical conductivity of CdS nanoparticles and PANi (EB) was found to be 1.5×10^{-6} S/cm and 4×10^{-4} S/cm respectively. The conductivity of PANi (EB)–CdS nanocomposite decreases slightly from 6.6×10^{-6} S/cm to 7.55×10^{-6} S/cm as content of CdS increases from 10 to 50% in PANi (EB) matrix.

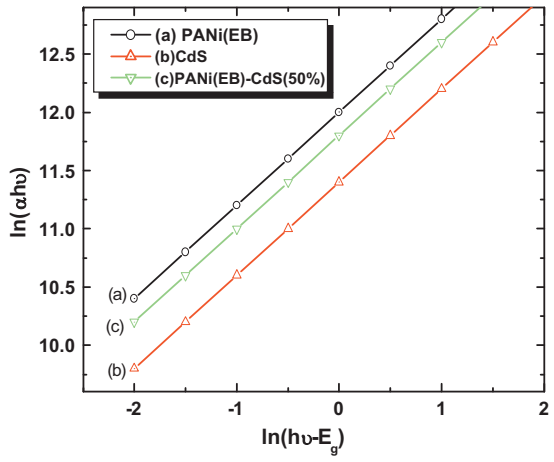

Fig. 6. Plot of $\ln(\alpha h\nu)$ versus $\ln(h\nu - E_g)$ (a) PANi (EB), (b) CdS and (c) PANi–CdS (50%) nanocomposites.

The thermo-emfs generated by the samples were measured in the 300–500 K temperature range.

The CdS shows n-type conduction, PANi (EB) and PANi–CdS (10–50%) composites shows p-type conduction. From the experimental observations it appeared that the temperature dependence of thermo power is approximately linear in the low temperature region whereas it deviated from the linear behavior at higher temperature and obeys power law dependence of the temperature. This is shown in Fig. 8. The non-linearity of the plots indicates nondegeneracy of the material whose thermo-electric power is proportional to nth power of the absolute temperature. For such semiconductors thermoelectric power is a weak function of the temperature and can be represented as [30]:

$$P = -\frac{K}{e}\left[r + \frac{5}{2}\right] + \ln\left\{\frac{2(2\pi m_d^* kT)^{3/2}}{nh}\right\}^3 \quad (4)$$

where $A = r + 5/2$ is a thermoelectric factor that depends on the various scattering mechanisms, m_d^* is the density of states effective mass and n is the carrier density. Eq. (4) can be solved for appropriate values of A and m_d^* and carrier density (n) were calculated for all the samples at different temperatures.

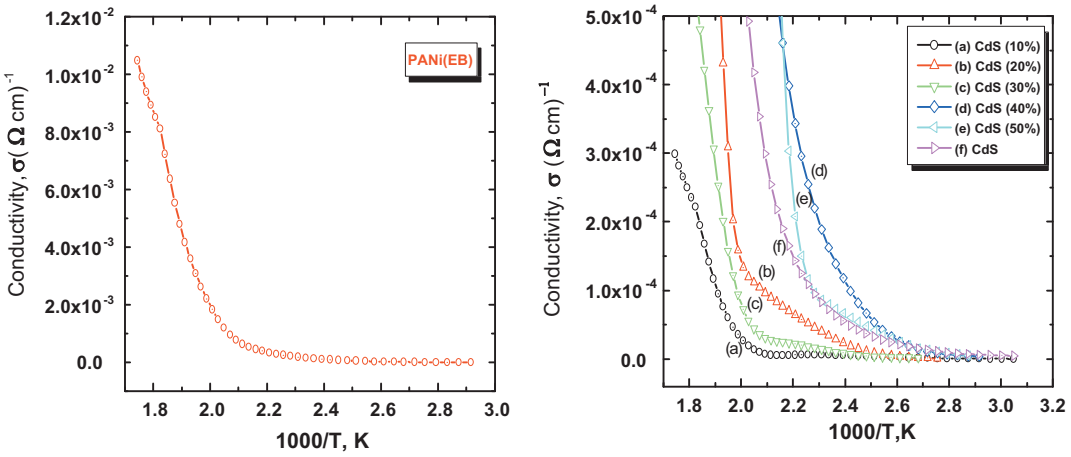

Fig. 7. Plot of dc electrical conductivity of PANi (EB), CdS and PANi–CdS (10–50%) nanocomposites as a function of inverse absolute temperature.

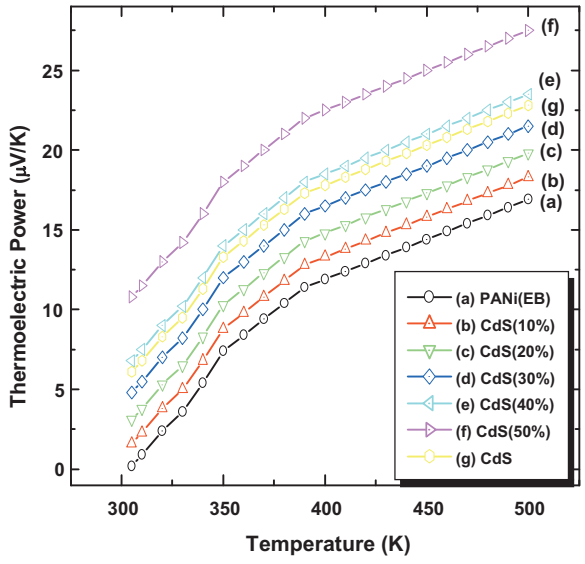

Fig. 8. Temperature dependence of thermoelectric power of PANi (EB), CdS and PANi–CdS (10–50%).

The charge carrier motilities (μ) were determined using the standard relation

$$\mu = \frac{\sigma}{n \cdot e} \tag{5}$$

Fig. 9 is a plot of the carrier density (n) and mobility (μ) as a function of the composites. It is seen that the carrier density and mobility are dependent functions of the temperature and materials compositions. These variations are analogous with that of the electrical conductivity variations. Further, the mobility increased with the applied temperature suggesting the presence of scattering mechanism associated with the inter-grain barrier height as proposed by Petriz [31]. The temperature dependent grain boundary mobility is related to the grain boundary poetical as [31]:

$$\mu = \mu_0 \exp\left(\frac{-\Phi_b}{kT}\right) \tag{6}$$

where Φ_b is the inter grain barrier potential and μ_0 is the pre exponential factor. The inter grain barrier potential is therefore

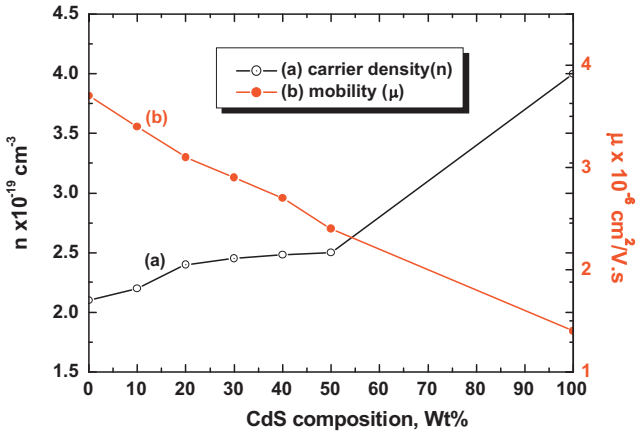

Fig. 9. Dependence of carrier density (n) and mobility (μ) on composition of CdS in PANi (EB).

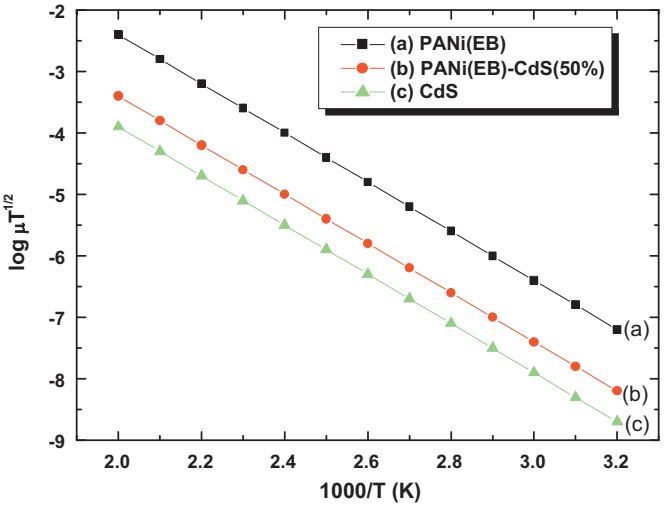

Fig. 10. Plot of log $\mu T^{1/2}$ with inverse temperature for: (a) PANi (EB), (b) PANi–CdS (50%) nanocomposites and (c) CdS.

determined from the variation of the log $\mu T^{1/2}$ versus $1000/T$ for all the samples and the values are 0.48–0.57 eV (Table 1). Fig. 10 is a representative case of such variation for film composition.

4. Conclusions

It has been shown for the first time that the films PANi–CdS nanocomposites were synthesized by spin coating technique. A change in the value of lattice parameter of CdS in the PANi–CdS composite was observed which also indicated the presence of interaction between CdS particles and PANi matrix. From FTIR spectra it is revealed that the characteristic absorption peaks of PANi (EB) shifted by significant amount into PANi–CdS nanocomposite, which indicate the different interfacial interactions between the CdS NPs and the PANi matrix. Study of field emission scanning electron microscopy revealed the synthesis of CdS nano particles of sizes ≈30–40 nm and their uniform dispersion in PANi matrix. The optical spectra revealed a high absorption coefficient of absorption and shift in absorption edge typically from 3.40 eV to 2.54 eV. The transitions are of direct type from band to band. The room temperature dc electrical conductivity of PANi (EB)–CdS (10–50%) nanocomposites is found to be in the range of 10^{-6} S/cm. Both grain boundaries scattering limited and hopping conduction mechanism are involved in the conduction process.

The measured thermoelectric power PANi (EB) and PANi–CdS (10–50%) nanocomposites is positive indicating large predominance of holes in the conduction process. The carrier density (n) and mobility (μ) are dependent functions of the temperature and film composition.

Acknowledgment

Authors (VBP) are grateful to DAE-BRNS, for financial support through the scheme no. 2010/37P/45/BRNS/1442.

References

[1] B.W.J.E. Beek, L.H. Slooff, M.N. Wienk, J.M. Kroon, R.A.J. Janseen, Hybrid solar cells using a zinc oxide precursor and a conjugated polymer, Adv. Funct. Mater. 15 (2005) 1703–1709.
[2] X.M. Sui, C.L. Shao, Y.C. Liu, Photoluminescence properties of highly dispersed ZnO quantum dots in polyvinyl pyrrolidone nanotubes prepared by a single capillary electrospinning, Appl. Phys. Lett. 87 (2005) 113–118.
[3] D.C. Olson, J. Piris, R.T. Colins, S.E. Shaheen, D.S. Ginley, Hybrid photovoltaic devices of polymer and ZnO nanofiber composites, Thin Solid Films 496 (2006) 26–29.
[4] Z.X. Xu, V.A.L. Roy, P. Stallinga, M. Muccini, S. Toffanin, H.F. Xiang, C.M. Che, High efficiency phosphorescent organic light-emitting diodes using carbazole-type triplet exciton blocking layer, Appl. Phys. Lett. 90 (2007) 223505–223509.
[5] G. Gustafsson, Y. Cao, G.M. Treacy, F. Klavetter, N. Colaneri, A. Heeger, Flexible light-emitting diodes made from soluble conducting polymers, Nature 357 (1992) 477–479.
[6] M.J. Sailor, E.J. Ginsburg, C.B. Gorman, A. Kumar, R.H. Grubbs, N.S. Lewis, Thin films of n-Si/poly-$(CH_3)_3$Si-cyclooctatetraene: conducting-polymer solar cells and layered structures, Science 249 (1990) 1146–1149.
[7] X. He, W. Qi, Ultrasonic irradiation: a novel approach to prepare conductive polyaniline/nanocrystalline TiO_2 composites, Chem. Mater. 14 (2002) 2158–2165.
[8] C. Danielle, S. Michelle, A. Ivo, Z. Aldo, Preparation and characterization of novel hybrid materials formed from $(Ti,Sn)O_2$ nanoparticles and polyaniline, Chem. Mater. 15 (2003) 4658–4665.
[9] J. Park, S. Park, A. Koukitu, O. Hatozaki, N. Oyarna, Electrochemical and chemical interactions between polyaniline and palladium nanoparticles, Synth. Met. 141 (2004) 265–269.
[10] R. Chandrakanthi, M. Careem, Preparation and characterization of CdS and Cu_2S nanoparticle/polyaniline composite films, Thin Solid Films 417 (2002) 51–56.
[11] S. Pethkar, R. Patil, J. Kher, K. Vijayarnohanan, Deposition and characterization of CdS nanoparticle/polyaniline composite films, Thin Solid Films 349 (1999) 105–109.
[12] M. Matsumura, T. Ohno, Concerted transport of electrons and protons across conducting polymer membranes, Adv. Mater. 9 (1997) 357–359.
[13] H. Yoneyama, N. Takahashi, S. Kuwabata, Catalytic asymmetric reaction of lithium ester enolates with imines, J. Chem. Soc. Chem. Commun. 2 (1999) 716–719.
[14] P.K. Khanna, S.P. Lonkar, V.V.V.S. Subbarao, K.-W. Jun, Polyaniline–CdS nanocomposite from organometallic cadmium precursor, Mater. Chem. Phys. 87 (2004) 49–53.
[15] D.Y. Godovsky, A.E. Varfolomeev, D.F. Zaretsky, R.L.N. Chandrakanthi, A. Kundig, C. Weder, W. Caseri, Preparation of nanocomposites of polyaniline and inorganic semiconductors, J. Mater. Chem. 11 (2001) 2465–2469.
[16] S.G. Pawar, S.L. Patil, M.A. Chougule, A.T. Mane, V.B. Patil, Synthesis and characterization of polyaniline: TiO_2 nanocomposites, Int. J. Polym. Mater. 59 (2010) 777–789.
[17] S.G. Pawar, S.L. Patil, M.A. Chougule, S.N. Acharya, V.B. Patil, Microstructural and optoelectronic studies on polyaniline: TiO_2 nanocomposite, Int. J. Polym. Mater. 60 (2011) 244–248.
[18] T.K. Sarma, A. Chattopadhyay, Reversible encapsulation of nanometer-size polyaniline and polyaniline–Au-nanoparticle composite in starch, Langmuir 20 (2004) 4733–4737.
[19] M.V. Kulkarni, A.K. Viswanath, R. Marimuthu, Synthesis and characterization of polyaniline doped with organic acids, J. Polym. Sci. A: Polym. Chem. 42 (2004) 2043–2049.
[20] Y. He, A novel emulsion route to sub-micrometer polyaniline/nano-ZnO composite fibers, Appl. Surf. Sci. 249 (2005) 1–6.
[21] H.C. Pant, M.K. Patra, S.C. Negi, A. Bhatia, S.R. Vadera, N. Kumar, Studies on conductivity and dielectric properties of polyaniline–zinc sulphide composites, Bull. Mater. Sci. 29 (2006) 379–384.
[22] H. Tang, Preparation and characterization of water-soluble CdS nanocrystals by surface modification of ethylene diamine, Mater. Lett. 59 (2005) 1024–1027.
[23] S.S. Kawar, B.H. Pawar, Synthesis and characterization of CdS n-type of semiconductor thin films having nanometer grain size, Chalcogenide Lett. 6 (2009) 219–225.
[24] S. Chandra, R.K. Pandya, Semiconductor photoelectrochemical solar cell, Phys. Status Solidi (a) 92 (1982) 415–419.
[25] V.B. Patil, S.G. Pawar, S.L. Patil, ZnO nanocrystalline thin films: a correlation of microstructural, optoelectronic properties, J. Mater. Sci. Mater. Electron. 41 (2010) 355–359.
[26] B.T. Raut, P.R. Godse, S.G. Pawar, M.A. Chougule, V.B. Patil, New method for fabrication of polyaniline–CdS sensor for H_2S gas detection, Measurements 45 (2012) 94–100.
[27] P.S. Nair, R. Revaprasadu, T. Radhakrishna, G.A. Kolawole, Preparation of CdS nanoparticles using the cadmium (II) complex of N,N'-bis(thiocarbamoyl)hydrazine as a simple single-source precursor, J. Mater. Chem. 11 (2001) 1555–1560.
[28] Y. Wada, H. Kuramoto, J. Anand, T. Kitamura, T. Sakata, Microwave-assisted size control of CdS nanocrystallites, J. Mater. Chem. 11 (2001) 1936–1940.
[29] A. Sekkina, A. Tawfik, Further studies on the temperature dependence of the electric and photovoltaic properties of CdSe thin films for solar cells, Thermochim. Acta 86 (1995) 431–435.
[30] G. Micocci, A. Tepore, R. Rella, P. Siciliano, Electrical and optical characterization of electron beam evaporated In_2Se_3 thin films, Phys. Status Solidi (a) 148 (1995) 431–443.
[31] R.L. Petriz, Theory of photoconductivity in semiconductor films, Phys. Rev. 104 (1956) 1508.